Research Report

Study on Hybrid Control Based on Reaction Null Space

Tokyo City University
Graduate School of Engineering
Mechanical Systems Engineering
Robotic Life Support Laboratory
1481214 Hiroki Sone
Advisor: Prof. Yoshikazu Kanamiya
Assoc. Prof. Daisuke Sato

June 3, 2015

Contents

List of Figures

List of Tables

Chapter 1

Introduction

Chapter 2

Hybrid Control Based on Reaction Null Space

In this chapter, we examine the hybrid control based on Reaction-Null Space method with simple planar three-link redundant manipulator and spatial seven-dof redundant manipulator.

2.1 Hybrid control based on Reaction Null Space

2.1.1 Reaction-Null Space based on the dynamics formulation

Reaction-Null Space (RNS) method is a reaction control for space robots, such as free-floating model and flexible-base model. In this method, we can treat the dynamic coupling between the end-link A, which referred to as the base as shown in Fig. 3.1, and the other links through the coupling inertia matrix described above. By controlling the dynamic coupling, the base can be traced the desired trajectory or can be decoupled from the influence of the other link dynamics. Reactionless motion control in space robots is used the second feature by using null-space of the coupling inertia matrix. On the other hand, for the purpose of hybrid control of the end-effector, we will use the former property of the dynamics coupling. Before describing this, we explain Reaction-Null Space formulation based on the equation of motion briefly.

The equation of motion of free-floating base model can be written in the following

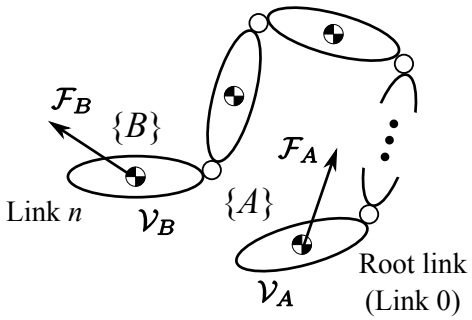

Fig. 2.1: Free-floating manipulator model.

form:

$$\begin{bmatrix} \boldsymbol{M}_A & \boldsymbol{M}_{Al} \\ \boldsymbol{M}_{Al}^T & \boldsymbol{M}_l \end{bmatrix} \begin{bmatrix} \dot{\mathcal{V}}_A \\ \ddot{\boldsymbol{\theta}} \end{bmatrix} + \begin{bmatrix} \mathcal{C}_A \\ \boldsymbol{c}_l \end{bmatrix} + \begin{bmatrix} \mathcal{G}_A \\ \boldsymbol{g}_l \end{bmatrix} = \begin{bmatrix} \boldsymbol{0} \\ \boldsymbol{\tau} \end{bmatrix} - \begin{bmatrix} \mathcal{F}_A + \boldsymbol{T}\mathcal{F}_B \\ \boldsymbol{J}_l^T \mathcal{F}_A \end{bmatrix} \tag{2.1}$$

where, $\mathcal{V}_A \in \mathbb{R}^6$ stands for the six-dimensional velocity of the end-link A, $\boldsymbol{\theta} \in \mathbb{R}^n$ is the joint coordinate vector. $\boldsymbol{M}_A \in \mathbb{R}^{6\times 6}$, $\boldsymbol{M}_{Al} \in \mathbb{R}^{6\times n}$, $\boldsymbol{M}_l \in \mathbb{R}^{n\times n}$ are submatrices of the inertia matrix. In particular, $\boldsymbol{M}_{Al}$ denote inertia properties related to the dynamics coupling between the end-link A and the other links. This matrix is referred to as the coupling inertia matrix. $\mathcal{C}_A \in \mathbb{R}^6$, $\boldsymbol{c}_l \in \mathbb{R}^n$ denote nonlinear force vector of the end-link A and the other links, $\mathcal{G}_A \in \mathbb{R}^6$, $\boldsymbol{g}_l \in \mathbb{R}^n$ denote gravity force vector of the end-link A and the other links. $\boldsymbol{\tau} \in \mathbb{R}^n$ stands for the joint torque, which is used for control input of the system. $\mathcal{F}_A = [\boldsymbol{f}_A \ \boldsymbol{m}_A] \in \mathbb{R}^6$, $\mathcal{F}_B = [\boldsymbol{f}_B \ \boldsymbol{m}_B] \in \mathbb{R}^6$ are six-dimensional force vector. One of these forces, namely $\mathcal{F}_B$, will be used later for appropriate constraint force for make a quasi-fixed base for hybrid control. $\boldsymbol{T} \in \mathbb{R}^{6\times 6}$, $\boldsymbol{J}_l \in \mathbb{R}^{6\times n}$ denote the pose matrix and Jacobian matrix.

(**??**) describes the two coupled equation of motion. Upper part represents the entire system dynamics w.r.t. the end-link A, which include entire mass and inertia properties:

$$\boldsymbol{M}_A \dot{\mathcal{V}}_A + \boldsymbol{M}_{Al} \ddot{\boldsymbol{\theta}} + \mathcal{C}_A + \mathcal{G}_A = -(\mathcal{F}_A + \boldsymbol{T}\mathcal{F}_B) \tag{2.2}$$

On the other hand, the lower part describes the dynamics of a "conventional" fixed-base manipulator, when the end-link B is fixed:

$$\boldsymbol{M}_{Al}^T \dot{\mathcal{V}}_A + \boldsymbol{M}_l \ddot{\boldsymbol{\theta}} + \boldsymbol{c}_l + \boldsymbol{g}_l = \boldsymbol{\tau} - \boldsymbol{J}^T \mathcal{F}_B \tag{2.3}$$

This manipulator is composed of all bodies except the end-link B; because the end-link B is the root, quantities $\boldsymbol{M}_l$, $\boldsymbol{c}_l$, $\boldsymbol{g}_l$, and $\boldsymbol{J}$ are those of the fix-ed-base manipulator.

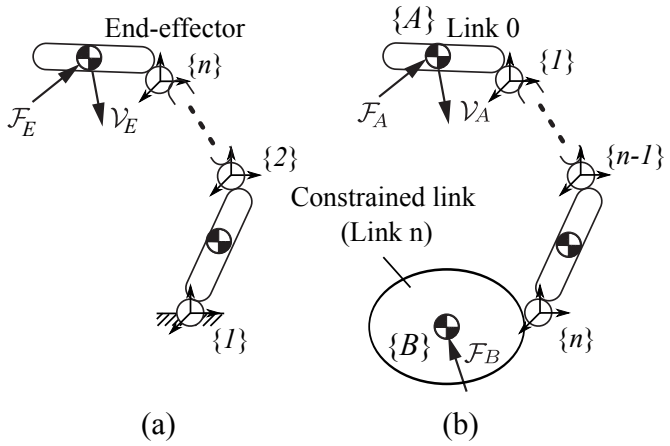

Fig. 2.2: This figure shows how to construct the control model based on the RNS-C for fixed-base manipulators: (a) real model and (b) control model.

It should be noted that the force and acceleration vector of the end-link A appear in the equation of motion (**??**). In addition, this equation also contain the joint acceleration term through the coupling inertia property. Hence, we can use this equation for hybrid control of the end-effector with explicit joint dynamics.

For the purpose of control of the end-link A, the reference joint acceleration can be obtained using Reaction-Null space manner:

$$\ddot{\boldsymbol{\theta}}^{ref} = \boldsymbol{M}_{Al}^{+}(\boldsymbol{S}^{\perp}\mathcal{F}_A^{ref} - \boldsymbol{M}_A\boldsymbol{S}\dot{\mathcal{V}}_A^{ref}) + \boldsymbol{M}_{Al}^{+}(\boldsymbol{T}\mathcal{F}_B - \mathcal{C}_A - \mathcal{G}_A) + \boldsymbol{P}_{RNS}\ddot{\boldsymbol{\theta}}_a \qquad (2.4)$$

2.1.2 Modeling of control model

In this section, we will describe how to adopt the RNS based control method for fixed-base manipulators. First, we display building the control model, which is based on free-floating systems for using RNS-C, for general n-link fixed-base manipulators in Fig. **??**.

Because, our aim is controlling of position and force of the end-effector, we set the reference frame $\{A\}$ onto the equivalent link of control model (Fig. **??** (b)). We will call this link as base link or simply, base. Note that the order of setting of local coordinates are reversed from the real model. In this case, as displayed in Fig. **??**, the control model is composed of $n+1$-link. On the other hand, the real model has only n links. Hence, there is one redundant link in the control model due to the constrained to the ground. If the real model is fixed-base manipulators, this redundant link does not have a physical meaning. Hence, the inertia of the link can be assigned arbitrary

values. However, even if this link does not have important role in the real model, because RNS-C is used the dynamic coupling between the base and other links, the inertia of this constrained link would affect entire motion of the manipulator. For this reason, we have to clarify the influence of the inertia on control systems. An theoretical and empirically verification will be described in Chapter **??**.

In order to obtain mechanically equivalence to control model, we have to apply a constraint force for making quasi-fixed base manipulator to the end-link B, which is displayed in Fig. **??** (b) as $\{B\}$. In this work, constraint force is obtained via Lagrange's method of undetermined multipliers as:

$$\mathcal{F}_B = \boldsymbol{\Lambda}\big(\boldsymbol{J}_c\boldsymbol{M}^{-1}(\boldsymbol{c}+\boldsymbol{g}-\boldsymbol{Q}) - \dot{\boldsymbol{J}}_c\dot{\boldsymbol{q}}\big) \tag{2.5}$$

$$\boldsymbol{\Lambda} = (\boldsymbol{J}_c\boldsymbol{M}^{-1}\boldsymbol{J}_c^T)^{-1} \tag{2.6}$$

$$\boldsymbol{Q} = \begin{bmatrix}\boldsymbol{0}\\ \boldsymbol{\tau}\end{bmatrix} \tag{2.7}$$

$$\boldsymbol{q} = \begin{bmatrix}\mathcal{V}_A\\ \dot{\boldsymbol{\theta}}\end{bmatrix} \tag{2.8}$$

where, $\boldsymbol{J}_c \in \mathbb{R}^{m_c\times(n+6)}$ stands for constraint Jacobian, m_c represents a degree of constraint.

In the following section, we will verify effectiveness of proposed method via numerical simulations.

2.2 Verification in three-link planar redundant manipulators

2.2.1 Applied model

In this section, we verify the proposed method in the three-link planar redundant manipulators. We display the real model and control model in Fig. **??**. In control model, the reference frame $\{A\}$ is attached in the equivalent end-effector as displayed in Fig. **??** (b). Note that we denote $(\hat{\circ})$ as parameters of control model in order to distinguish between the real model and control one. The parameters of the real model and control model are displayed in Table **??**. Determination of the inertia of constrained link will be described in next chapter.

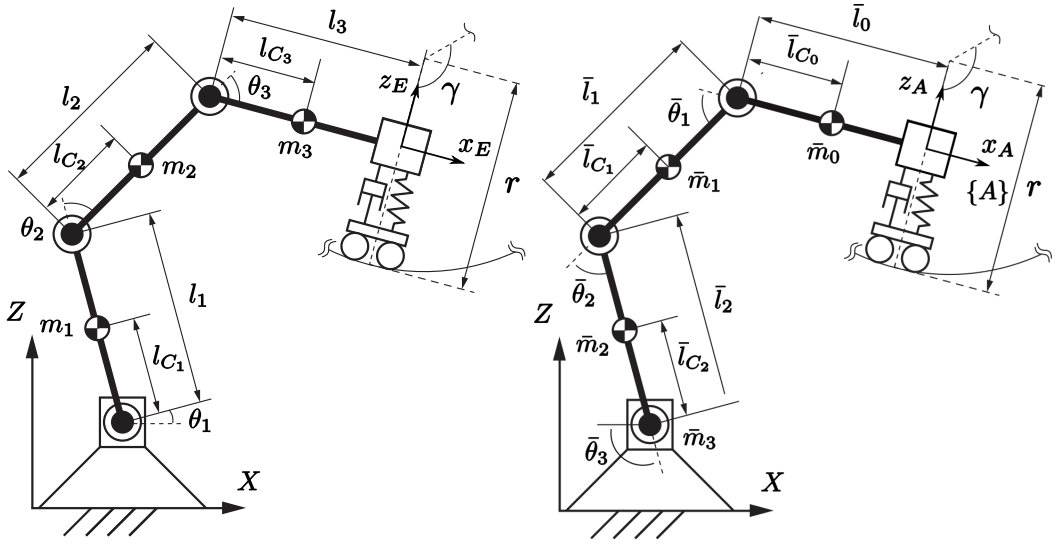

Fig. 2.3: 3R planar redundant manipulator: (a) real model and (b) control model. The parameters in the control model is represented using bar.

Table 2.1: Model parameters

	Real model		Control model	
i	Mass $m_i[kg]$	Length $l_i[m]$	Mass $\bar{m}_i[kg]$	Length $\bar{l}_i[m]$
0	–	–	10	1
1	10	1	10	1
2	10	1	10	1
3	10	1	1.0×10^5	0

Compensation of the dynamic coupling of rotation

In this model, we regard position of the end-effector as control quantity. Hence, orientation does not deal in this work. However, from the equation of motion (**??**), we can confirm that there is a dynamic coupling between the tranlational dynamics and rotational one in follows:

$$\boldsymbol{M}_v\dot{\boldsymbol{v}}_A + \boldsymbol{M}_{v\omega}\dot{\boldsymbol{\omega}}_A + \boldsymbol{M}_{vl}\dot{\boldsymbol{\theta}} + \boldsymbol{c}_v + \boldsymbol{g}_v = -\boldsymbol{T}_v[\boldsymbol{f}_B^T \; m_B]^T + [\boldsymbol{f}_A^T \; m_A]^T \tag{2.9}$$

Because of large noise of acceleration measurement, it is not appropriate to use sensor dates. Hence, we evaluate this coupling from the equation of motion. From (**??**), the

angular acceleration of the base can be obtained in the following form:

$$\dot{\boldsymbol{\omega}}_A = -M_\omega^{-1}(\boldsymbol{M}_{v\omega}^T \dot{\boldsymbol{v}}_A + \boldsymbol{M}_{\omega l}\ddot{\boldsymbol{\theta}} + c_{\omega,z} + g_{\omega,z} - \boldsymbol{T}_\omega[\boldsymbol{f}_B^T \; m_B]^T) \tag{2.10}$$

By substituting (**??**) into (**??**) and solving the joint acceleration, the reference joint acceleration can be formulated as:

$$\ddot{\tilde{\boldsymbol{\theta}}}^{ref} = \tilde{\boldsymbol{M}}_{vl}^+(\boldsymbol{S}^\perp \boldsymbol{f}_A^{ref} - \tilde{\boldsymbol{M}}_v \boldsymbol{S}\dot{\boldsymbol{v}}_A^{ref} - \tilde{\boldsymbol{M}}_v \dot{\boldsymbol{S}}\bar{\boldsymbol{v}}_A) + \tilde{\boldsymbol{M}}_{vl}^+(\tilde{\boldsymbol{T}}\boldsymbol{f}_B - \tilde{\boldsymbol{c}}_A - \tilde{\boldsymbol{g}}_A) \tag{2.11}$$

$$\tilde{\boldsymbol{M}}_v = \boldsymbol{M}_v - \boldsymbol{M}_{v\omega}M_\omega^{-1}\boldsymbol{M}_{v\omega} \in \mathbb{R}^{2\times 2} \tag{2.12}$$

$$\tilde{\boldsymbol{M}}_{vl} = \boldsymbol{M}_{vl} - \boldsymbol{M}_{v\omega}M_\omega^{-1}\boldsymbol{M}_{\omega l} \in \mathbb{R}^{2\times 3} \tag{2.13}$$

$$\tilde{\boldsymbol{c}}_A = \boldsymbol{c}_A - \boldsymbol{M}_{v\omega}M_\omega^{-1}c_{\omega,z} \in \mathbb{R}^2 \tag{2.14}$$

$$\tilde{\boldsymbol{g}}_A = \boldsymbol{g}_A - \boldsymbol{M}_{v\omega}M_\omega^{-1}g_{\omega,z} \in \mathbb{R}^2 \tag{2.15}$$

$$\tilde{\boldsymbol{T}}_v = \boldsymbol{T}_v - \boldsymbol{M}_{v\omega}M_\omega^{-1}\boldsymbol{T}_\omega \tag{2.16}$$

where, note that $\tilde{(\circ)}$ is represented quantities including the dynamic coupling of rotation.

Parameter transformation between the real and control model

If we set the local coordinate frames in each joint as shown in Fig. **??**, the relationship between the real model and control model is obtained as:

$$\begin{aligned}[x_E, z_E, \phi_E]^T &= [\bar{x}_A, \bar{z}_A, -\bar{\phi}_A]^T \\ \boldsymbol{\theta} &= -[\bar{\theta}_3, \bar{\theta}_2, \bar{\theta}_1]^T \\ \dot{\boldsymbol{\theta}} &= -[\dot{\bar{\theta}}_3, \dot{\bar{\theta}}_2, \dot{\bar{\theta}}_1]^T \\ \boldsymbol{\tau} &= -[\bar{\tau}_3, \bar{\tau}_2, \bar{\tau}_1]^T\end{aligned} \tag{2.17}$$

where, ϕ_A, $\bar{\phi}_E$ denote orientation of the base and the end-effector, respectively.

2.2.2 Verification via numerical simulation

We adopted the initial configuration as $\boldsymbol{\theta}(t_0) = [-105, -60, -60]^T$ deg, desired motion is repeat motion tracking a circular arc with radius $r = 0.707$ m as displayed in Fig. **??**. The trajectory are obtained via fifth-order nominal polynomial function. In addition, we define x-axis is the direction for position and z-axis is the force control direction w.r.t. the base attached frame. Hence, the directions of two reference input is orthogonal geometrically. Force trajectory are 10 N with fifth-order polynomial

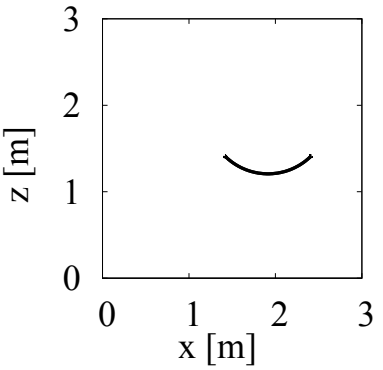

Fig. 2.4: Desired circular arc.

function. Note that we assume interaction is point contact and contact model is built via simple linear spring-damper system [12] as:

$$f_{Az} = k_n \delta_n + d_n \dot{\delta}_n \tag{2.18}$$

where, $k_n = 5.0 \times 10^4$ N/m, $d_n = 5.0 \times 10^2$ Ns/m are stiffness and viscosity of the contact surface, δ_n, $\dot{\delta}_n$ denote penetration of the position and velocity, which are namely relative position and velocity between the base and surface. Note that we assume that there is no frictional force for simplicity.

Control references of position and force control are obtained as feedback systems:

$$v_{A,x}^{ref}(t) = \dot{v}_{A,x}^{des}(t) + k_{d,x}(v_{Ax}^{des}(t) - v_{A,x}) + k_{p,x}(x_{A,x}^{des}(t) - x_{A,x}) \tag{2.19}$$

$$f_{A,z}^{ref}(t) = f_{A,z}^{des}(t) + k_{fz}(f_{A,x}^{des}(t) - f_{A,z}) \tag{2.20}$$

where, we obtain the feedback gains as $k_{d,x} = 10$ s^{-1}, $k_{p,x} = 100$ s^{-2}, $k_{f,z} = 5$ N.D., respectively. Simulation time, sampling time are 6 s, 1 ms. Note that we only focus on the particular components without null-space control.

The desired path and simulation results are displayed in Fig. **??** and Fig. **??**. From the results, we can observed that the maximum error of position tracking is 0.2 mm and force error is 5 mN. Therefore, we can concluded that the proposed method has sufficiently high accuracy and effectiveness.

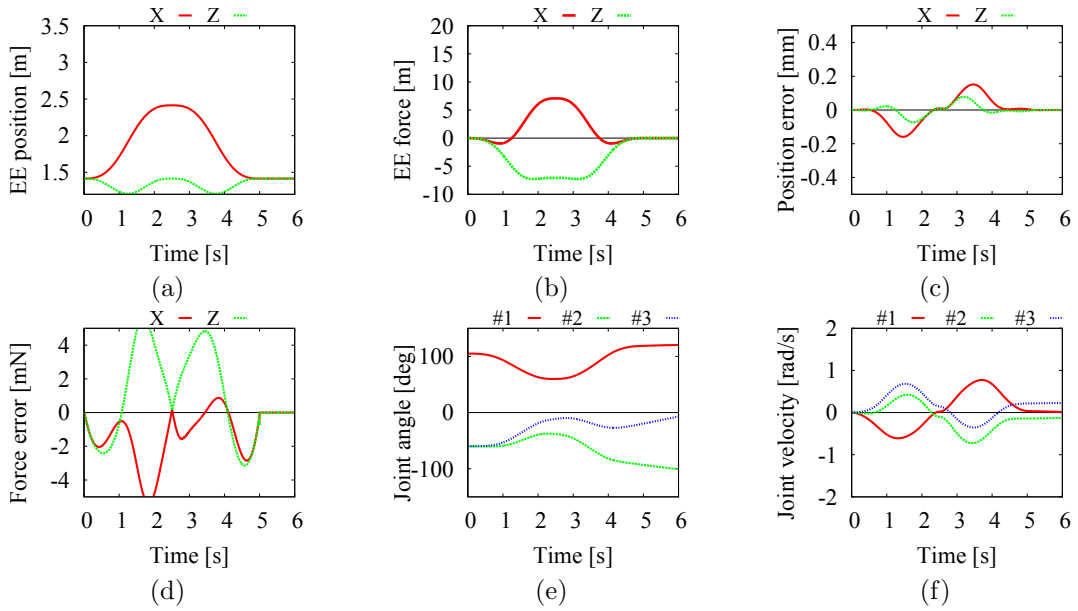

Fig. 2.5: Simulation results for position and force with particular-solution control torque only: (a) - (d): task-space quantities; (e)-(f): joint variables.

2.3 Verification in seven-dof spatial redundant manipulator

2.3.1 Applied model

In this section, we verify effectiveness of the proposed method in a seven-dof spatial redundant manipulator. The applied model is DLR (German space Agency) Light weight arm. We display the kinematic structure of the applied model in Fig. **??**. Control model is constructed as displayed in Fig. **??** (b) and the local coordinates are set as reversed order.

2.3.2 Verification via numerical simulation

With above manipulator model, we verify effectiveness of the proposed control law. CG image is displayed in Fig. **??**. The desired motion is repeat motion for y-direction in the end-effector attached frame as shown in Fig. **??**. On the other hand, force control is conducted for z-direction in the same frames. The reference force trajectory was obtained via fifth-order polynomial function from 0 to 5 N. Initial configuration was set as $[0, -20, 0, 100, 0, 10, 0]^T$ deg, simulation time and sampling time were 5 s

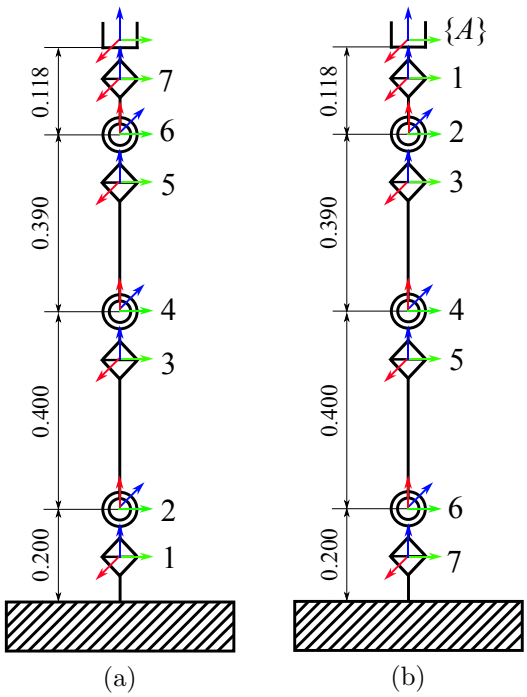

Fig. 2.6: Kinematic structure of the 7R redundant manipulator: (a) real model and (b) control model.

and 5 ms. The parameters of contact surface are same as the planar case.

The simulation results are displayed in Fig. **??**, Fig. **??**. From the results, we can confirm that the maximum position error was 0.2×10^{-6} m and force error was 0.5 mN.

In addition, we conducted another motion, such that x-directional motion, with same initial configuration and conditions. From the results, joint velocity is remained even if the end-effector motion is stopped. This is a nature of using pseudoinverse control due to non-integrability. We will discuss this redundant motion in the next chapter.

2.4 Summary

In this chapter, we verified Reaction-Null Space based hybrid control of redundant manipulators via numerical simulations. We dealt with simple three-link redundant manipulator and seven-dof spatial redundant manipulator for applied models. From the results, we can conclude that RNC-C is feasible in general manipulator model.

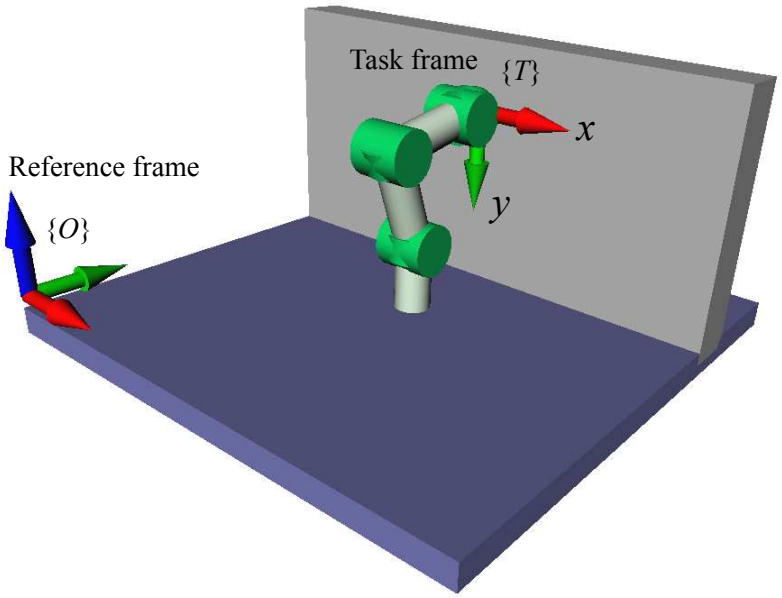

Fig. 2.7: Dynamic simulator of the seven-dof redundant manipulator. x and y-direction in the task frame $\{T\}$ are position controlling direction.

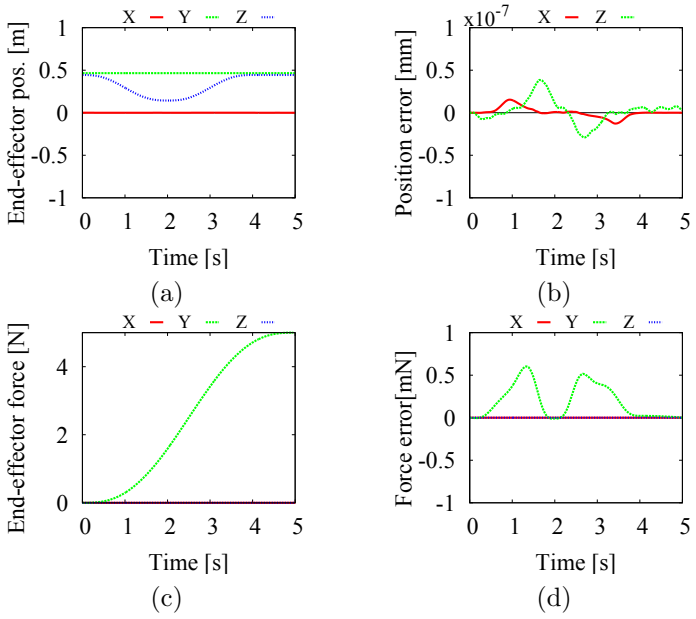

Fig. 2.8: Simulation results of z-direction path tracking: These figures show that the manipulator end-effector can follow the desired position/force trajectories.

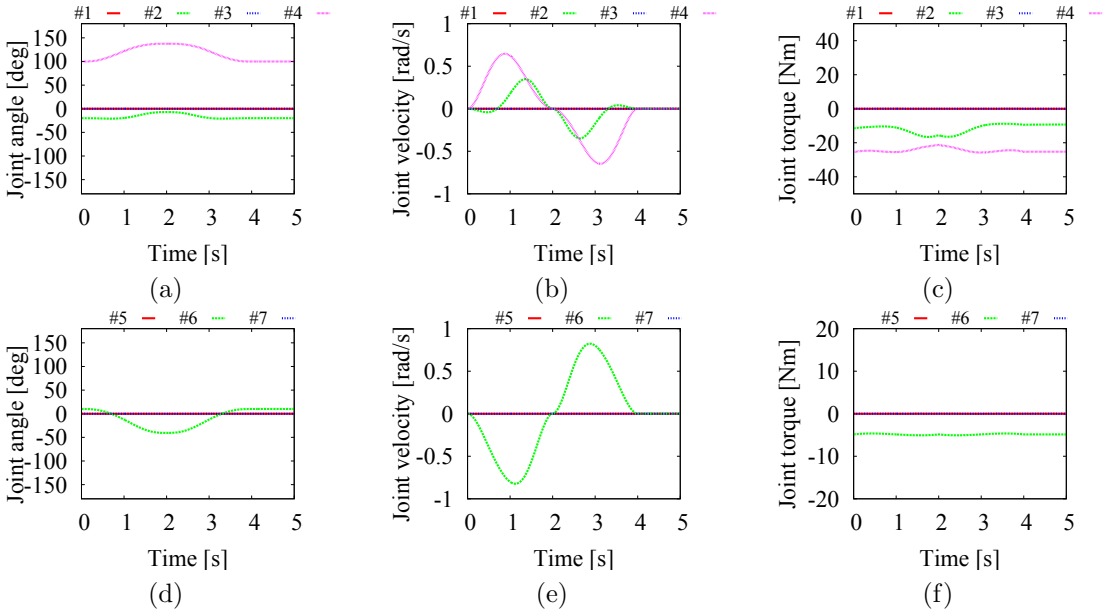

Fig. 2.9: Simulation results of x-direction path: (a)-(c): positioning subchain; (d)-(f): wrist subchain. In this case, because the motion is restricted onto the y-z plane, the manipulator is almost same as planar and nonredundant model.

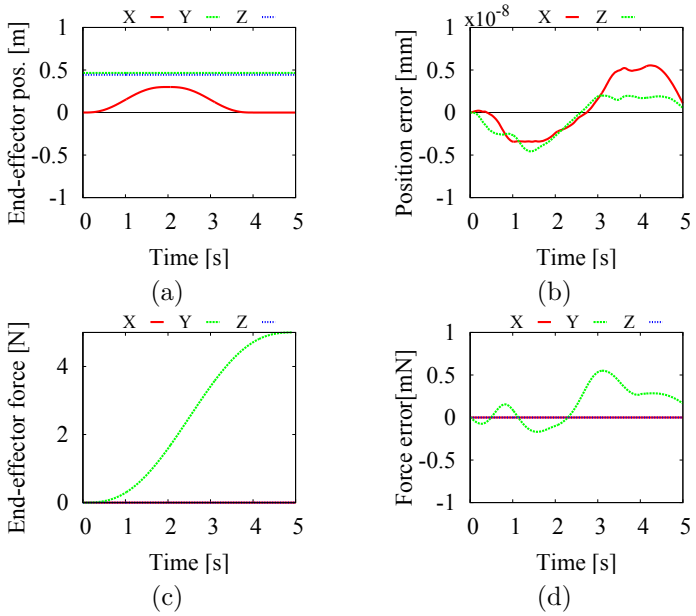

Fig. 2.10: Simulation results of x-direction path tracking: This figures show that the manipulator end-effector can follow the desired position/force trajectories.

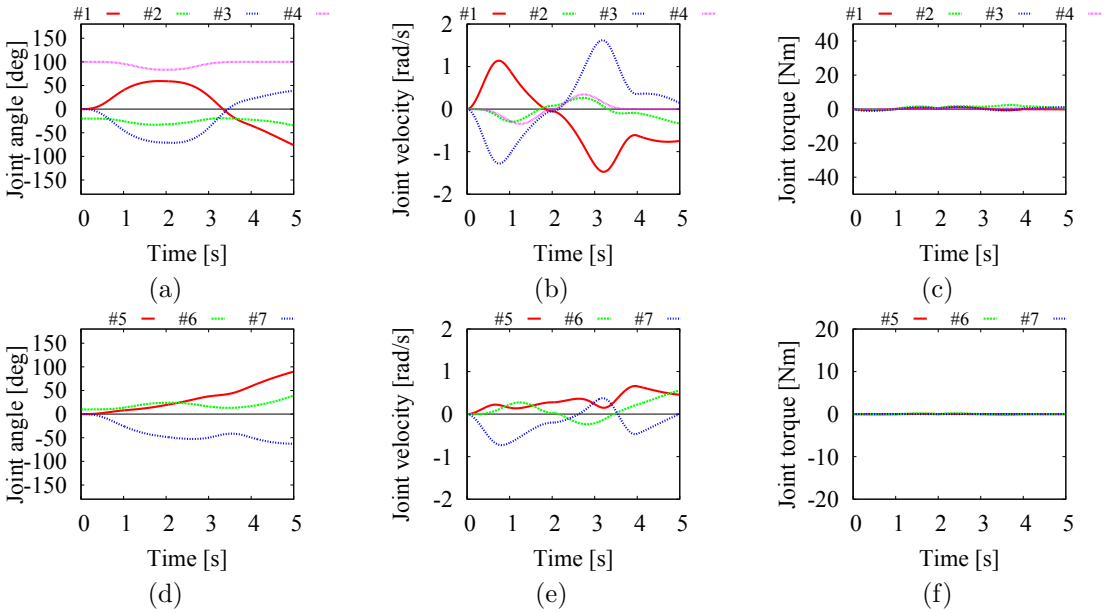

Fig. 2.11: Simulation results of x-direction path: (a)-(c): positioning subchain; (d)-(f): wrist subchain. Compared to the results of Fig. **??**, because the motion of manipulator is over y-z plane, redundant motion can be observed caused by non-integrability of pseudoinverse.

Chapter 3

Joint Motion Analysis with Redundant Manipulators

In this section, we will focus on joint motion of redundant manipulators under Reaction Null Space method. In particular, it is not clarified that influence of the inertia parameters of the constrained on joint motion. From this analysis, in a specific situation, the motion under Reaction Null Space coincides the motion under minimum acceleration norm with resolved acceleration control. In addition, we examine joint motion with well-known redundancy resolution technique, so-called *Operational Space Formulation* (OS) with inertia-weighted pseudoinverse.

In controlling redundant manipulators under acceleration level, there is a problem with instability of joint motion [13, 14]. To this problem, we propose a stabilizing method by using minimum velocity norm derived from momentum conservation law.

3.1 Influence of inertia parameters of the constrained link

As described in previous section, control model is composed of $n+1$ links. However, because real model have only n links, there is a redundant link in control model compared to real model. This link is used for making quasi-fixed base via an appropriate constraint force. This link havs meanings as ground when the model is completely fixed-base manipulator, or upper bodies when the model is a humanoid robot. And of course, if the model is a free-floating manipulator, such that space robots, we can also apply this inverted formulation to this model.

Among them, we focus on the case of completely fixed-base manipulator in this

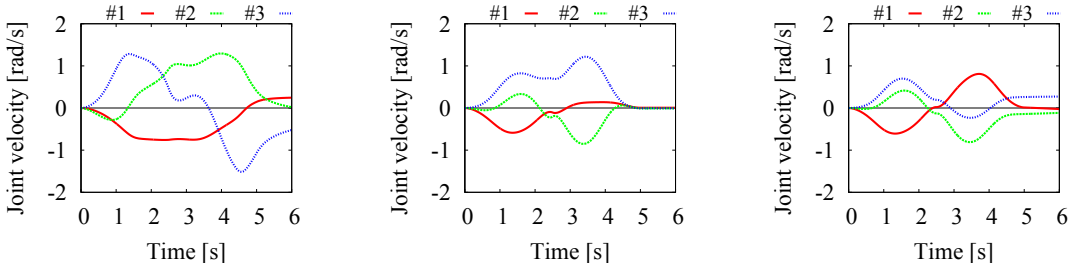

Fig. 3.1: Time profile of joint velocity under the circular arc trajectory tracking with some mass parameters of constrained link in the three-dof planar redundant manipulator: (a) 10 kg, (b) 100 kg and (c) 1000 kg.

section. In this case, the inertia parameters of the constrained link does not have a physical meaning because there is no parameters in real models. Therefore, this parameters can be assigned arbitrary values. However, because Reaction Null Space is the method using the dynamics coupling between the end-link A and the other links, this parameters affect joint motion through the constrained force. In the verification in Chapter **??**, we adapt a relatively large value for this parameter because of joint instability problem described in follows.

In this section, we will verify influence on joint motion when the inertia parameters of the constrained link are varied.

3.1.1 Planar three-dof redundant manipulator

In this section, we will verify the above influence in the planar three-dof redundant manipulator used in Chapter **??**. The geometric and inertia parameter are basically same as the previous one. We adapt the mass of the constrained link as $\bar{m}_3 = 10, 100, 1000$ kg. Also inertia moment are varied related to the mass parameter with same ratio. In addition, in order to focus on the joint motion, we assume that there is no interaction between the manipulator and an environment without loss of generality. The desired trajectory is the circular arc with same conditions in Chapter **??**.

We show time profiles of the joint velocity in Fig. **??**. From the results, it can be observed that joint motion are changed with increasing the inertia parameters. And also we can show that rate of change of joint velocity is reduced with large inertia parameters. In order to provide more clear inspection, we divide the null

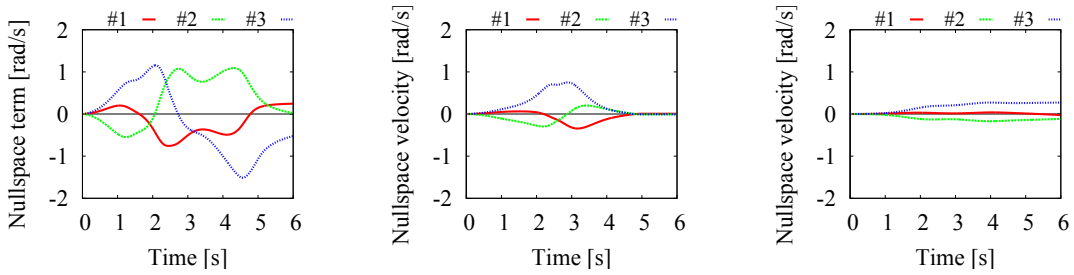

Fig. 3.2: Null-space velocity under the circular arc trajectory tracking in the three-dof planar redundant manipulator: (a) 10 kg, (b) 100 kg and (c) 1000 kg.

space velocity from joint velocity by using projection matrix of the Jacobian matrix. From the results, which are shown in Fig. **??**, the change ratio of null space velocity is reducing with increasing inertia parameters of the constrained link.

Seven-dof spatial redundant manipulator

We verify the influence in seven-dof spatial redundant manipulator for the same purpose in planar case. We choose the applied model as same model which was dealt in Chapter **??**. Besides, the desired motion trajectory and simulation condition are also same one in Chapter **??**. Note that we do not consider interaction to environments because we focus on only joint motion.

The results are shown in Fig. **??** with inertia parameters $\bar{m}_7 = 1, 10, 100$ kg. These figure represent the time profile of joint velocity. From the results, we can see that joint motion is affected by the inertia parameters of the constrained link. Besides, from the Euclidean norm of the null space velocity, as shown in Fig. **??**, rate of change of the null-space velocity is also reduced by increasing the inertia parameters of the constrained link in the spatial model.

In summary, we can conclude that the inertia parameters of the constrained link affect joint motion. In particular, the rate of change of the null-space velocity is reduced by increasing that parameters.

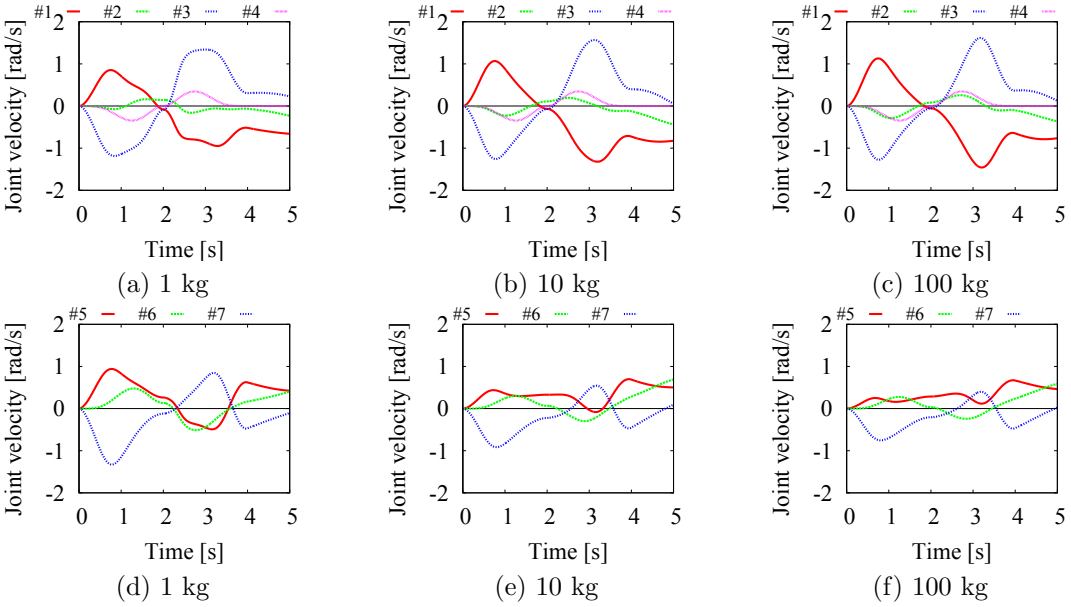

(a) 1 kg (b) 10 kg (c) 100 kg

(d) 1 kg (e) 10 kg (f) 100 kg

Fig. 3.3: Time profile of joint velocity under the straight trajectory tracking in the seven-dof spatial redundant manipulator with some inertia parameters: (a)-(c): positioning subchain (joint 1-4) and (d)-(f): wrist subchain (joint 5-7).

3.2 Comparison analysis of joint motion with representative redundancy resolution

In redundant manipulators, because there is infinity solution to realize desired motions of the end-effector, it is important to use appropriate resolution technique. In this section, we verify representative resolution techniques, such that resolved acceleration (RA-C) with minimum acceleration norm, Operational Space Formulation (OS-C) with inertia-weighted pseudoinverse and Reaction-Null Space (RNS-C), with focusing on joint motions.

3.2.1 Redundancy resolution

Here, before verifying the motion, we will explain RA-C and OS-C briefly.

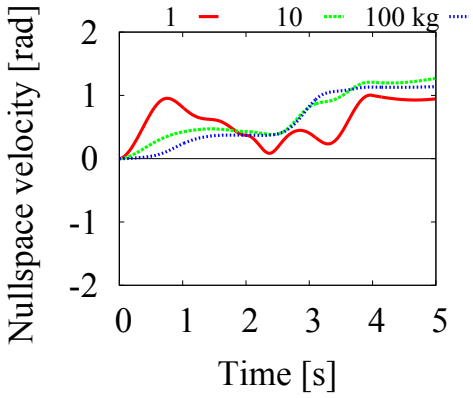

Fig. 3.4: Euclidean norm of the null-space velocity.

Resolved acceleration control [15]

RA-C is a control method based on the kinematic constraint at acceleration level. The reference joint acceleration can be obtained in the following form:

$$\ddot{\boldsymbol{\theta}}^{ref} = \boldsymbol{J}^{+}(\dot{\mathcal{V}}_e^{ref} - \dot{\boldsymbol{J}}\dot{\boldsymbol{\theta}}) + \boldsymbol{P}_J\ddot{\boldsymbol{\theta}}_a^{ref} \tag{3.1}$$

where, $\boldsymbol{J} \in \mathbb{R}^{6\times n}$ stands for the Jacobian matrix of the end-effector, $\boldsymbol{P}_J \in \mathbb{R}^{n\times n}$ is a projector into the null-space of the Jacobian matrix, $\ddot{\boldsymbol{\theta}}_a \in \mathbb{R}^n$ is an arbitrary vector with acceleration level. If we adopt $\ddot{\boldsymbol{\theta}}_a = \mathbf{0}$, the solution of minimum acceleration norm can be obtained. This motion seems to be relatively stable compared to other motions form redundancy resolution techniques.

Operational Space Formulation [16]

OS-C is the basic formulation for force control, such that hybrid control and impedance control. This formulation is based on the D'Alembert's principle and Gauss's principle [17]. In this formulation, control input is obtained as joint torque as:

$$\boldsymbol{\tau}^{ref} = \boldsymbol{J}^T(\boldsymbol{M}_e\boldsymbol{S}\dot{\mathcal{V}}_e^{ref} + \mathcal{C}_e + \mathcal{G}_e + \boldsymbol{S}^{\perp}\mathcal{F}_e^{ref}) + (\boldsymbol{E} - \boldsymbol{J}^T\boldsymbol{J}_M^{\#T})\boldsymbol{\tau}_a^{ref} \tag{3.2}$$

$$\boldsymbol{M}_e = (\boldsymbol{J}\boldsymbol{M}^{-1}\boldsymbol{J}^T)^{-1} \tag{3.3}$$

$$\mathcal{C}_e = \boldsymbol{J}_M^{\#T}\boldsymbol{c} - \boldsymbol{M}_e\dot{\boldsymbol{J}}\dot{\boldsymbol{\theta}} \tag{3.4}$$

$$\mathcal{G}_e = \boldsymbol{J}_M^{\#T}\boldsymbol{g} \tag{3.5}$$

$$\begin{aligned}\boldsymbol{J}_M^{\#} &= \boldsymbol{M}^{-1}\boldsymbol{J}^T\boldsymbol{M}_e \\ &= \boldsymbol{M}^{-1}\boldsymbol{J}^T(\boldsymbol{J}\boldsymbol{M}^{-1}\boldsymbol{J}^T)^{-1}\end{aligned} \tag{3.6}$$

where, $\boldsymbol{M}_e \in \mathbb{R}^{6\times6}$, $\mathcal{C}_e$, $\mathcal{G}_e \in \mathbb{R}^6$ are inertia matrix, the nonlinear and gravity force vector w.r.t. the operational point i.e. the end-effector. $\boldsymbol{J}_M^{\#}$ denotes inertia-weighted pseudoinverse, which provide the minimum weighted norm solution. In velocity level control, this solution provides minimum instantaneous kinetic energy.

In addition, the above formulation can be represented in the acceleration form with (**??**) and $\boldsymbol{\tau} = \boldsymbol{M}\ddot{\boldsymbol{\theta}} + \boldsymbol{c} + \boldsymbol{g} - \boldsymbol{J}^T\mathcal{F}_e$ in the following form:

$$\ddot{\boldsymbol{\theta}}^{ref} = \boldsymbol{J}_M^{\#}(\dot{\mathcal{V}}_e^{ref} - \dot{\boldsymbol{J}}\dot{\boldsymbol{\theta}}) + \boldsymbol{M}^{-1}(\boldsymbol{E} - \boldsymbol{J}^T\boldsymbol{J}_M^{\#T})(\boldsymbol{\tau}_a^{ref} - (\boldsymbol{c} + \boldsymbol{g})) \tag{3.7}$$

From above formulation, we can see that the nonlinear and gravity term affect redundant motion. Indeed, if we use (**??**) straightforwardly to redundant manipulator, joint motion cannot be stopped under gravity environment, ever if the gravity term w.r.t. operational point is compensated correctly. An example is shown in Fig. **??**. We can see an cyclic motion induced by gravity from the results.

3.2.2 Comparison via numerical simulation

Here, we compare the above redundancy resolutions via numerical simulations. In this case, we also adopt planar three-dof redundant manipulator and seven-dof spatial redundant manipulator as the applied model. Also, we only deal with position control of the end-effector because of focusing on joint motion. In the case of RNS-C, we choose sufficiently large values for the inertia parameters of the constrained link to reduce redundant motion. Note that we assume zero gravitational environment, because in the case of OS-F, the joint motion will be unstable due to the reason mentioned above.

Planar three-dof redundant manipulator

We verified in the planar model. The model parameters are adopted as same values in previous chapter. Initial configuration is set as $\boldsymbol{\theta}(t_0) = [105, -60, -60]^T$ deg. The desired trajectories are circular arc described in Chapter **??** and straight line to the point $[x(t_0) - 2,\ y(t_0) - 1]^T$ m.

We show the results in the case of circular trajectory tracking in Fig. **??**. It must be noted that, from the results, the motion under RNS-C coincides that under RA-C completely. Compared to these motions, it can be observed that the motion under OS-C has relatively large rate of change of the joint velocity. In addition, when the end-effector velocity becomes zero ($t = 2.5$ s), joint velocity under OS-C has quite

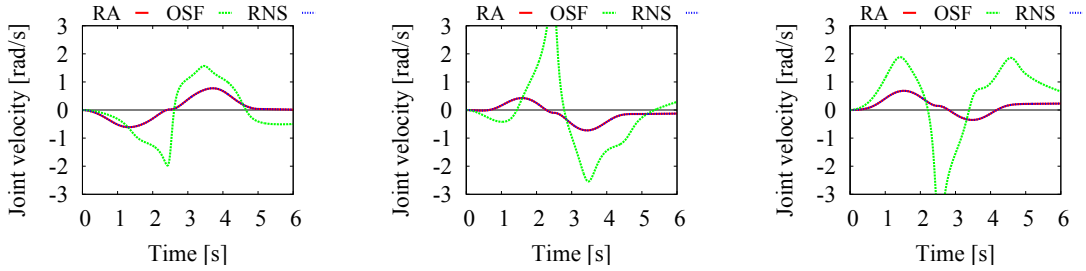

(a) Joint 1 (b) Joint 2 (c) Joint 3

Fig. 3.5: Simulation results of each joint velocity under circle path tracking. It can be observed that the joint motion of RNS is same as RA.

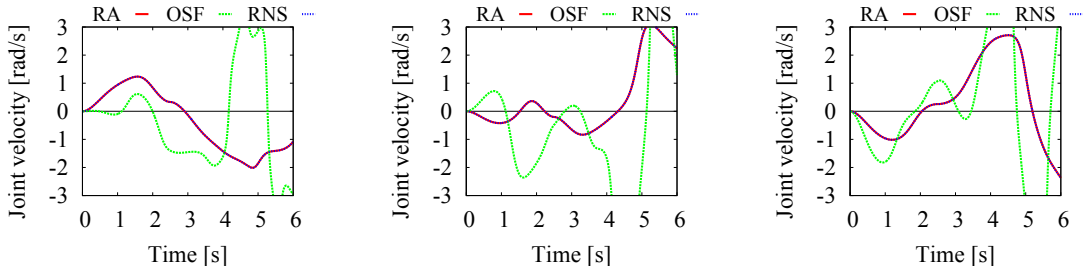

(a) Joint 1 (b) Joint 2 (c) Joint 3

Fig. 3.6: Simulation results of each joint velocity under straight line path tracking. It can be observed that the joint motion of RNS is same as RA.

large values. On the other hand, in the case of RNS-C or RA-C, joint velocity becomes small values. This is a main deference between the motion of RNS-C (or RA-C) and OS-C. This results can be seen in the case of straight line trajectory tracking as shown in Fig. **??**. From these results, we would conclude that RNS-C has a advantage in the perspective of joint motion stability compared to OS-C.

Seven-dof spatial redundant manipulator

Here, we examine the joint motion in seven-dof spatial redundant manipulator. In this case, we also focus on only joint motion without considering gravity and interaction to the environments. We adopt the desired trajectory as the x-directional straight line mentioned in Chapter **??**. Simulation conditions are also same as the previous ones. we show the obtained results in Fig. **??**. From these results, the motion under RNS-C also coincides that under RA-C as the results of planar case.

Finally, we can assume that the motion under RNS-C coincides that under RA-C in general manipulator model. Next section, we will discuss this results in the

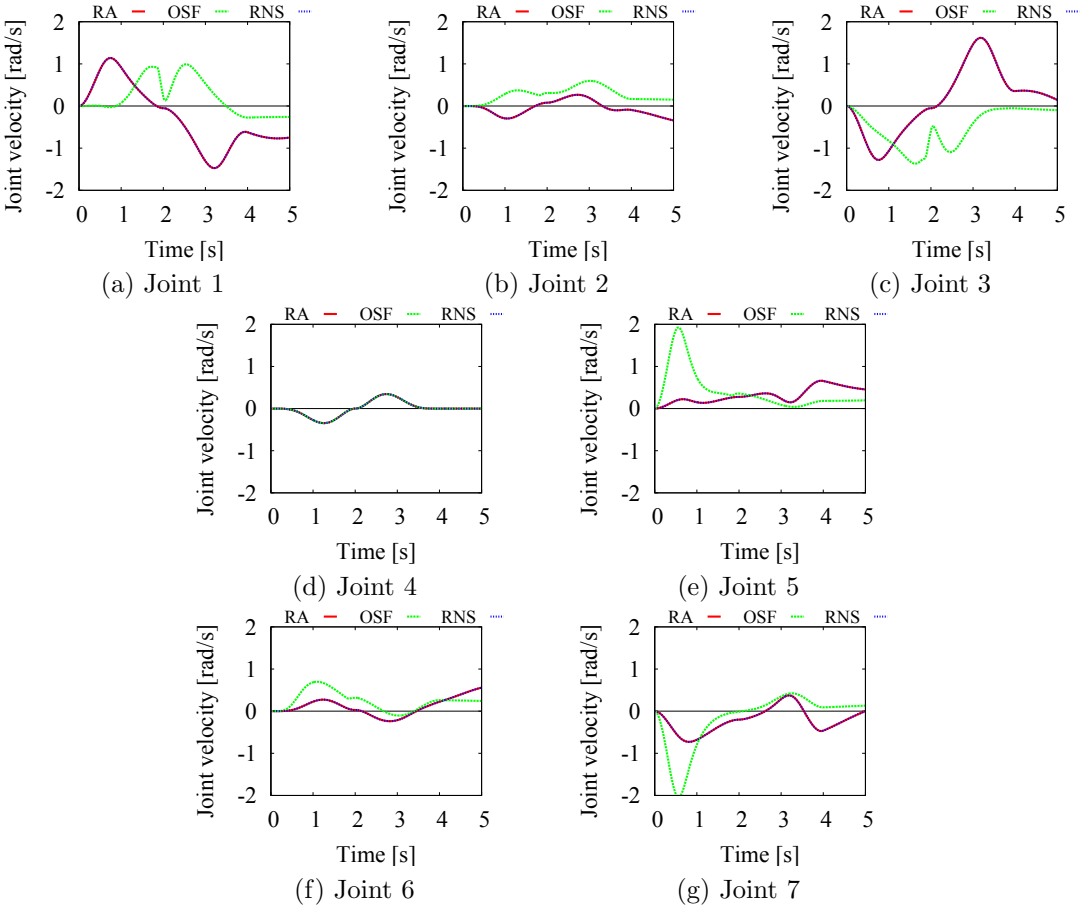

(a) Joint 1 (b) Joint 2 (c) Joint 3

(d) Joint 4 (e) Joint 5

(f) Joint 6 (g) Joint 7

Fig. 3.7: Comparison results in the seven-dof redundant manipulator under straight line path tracking. In the case of spatial manipulator, the joint motion under the RNS-C is also same as the motion of RA.

perspective of mathematical points.

3.3 Analysis of joint motion under RNS-C

3.3.1 Kinematic constraint of the end-effector acceleration

Before describing the feature of RNS-C joint motion, we should explain kinematic constraint of fixed-base manipulator (real model) at acceleration level. Acceleration of the end-effector is related to the joint acceleration (and also joint velocity) via the following kinematics constraint:

$$\dot{\mathcal{V}}_e = \boldsymbol{J}\ddot{\boldsymbol{\theta}} + \dot{\boldsymbol{J}}\dot{\boldsymbol{\theta}}, \tag{3.8}$$

Note that this constraint must be fulfilled regardless of absence of external forces and differs of control methods. From (**??**), when the desired acceleration of the end-effector is obtained, the joint acceleration which fulfill the above constraint can be obtained via pseudoinverse matrix of the Jacobian matrix as:

$$\ddot{\boldsymbol{\theta}}^{ref} = \boldsymbol{J}^{+}(\dot{\mathcal{V}}_e - \dot{\boldsymbol{J}}\dot{\boldsymbol{\theta}}) + \boldsymbol{P}_J\ddot{\boldsymbol{\theta}}_a \tag{3.9}$$

where, $\boldsymbol{P}_J = \boldsymbol{E} - \boldsymbol{J}^{+}\boldsymbol{J} \in \mathbb{R}^{n\times n}$ is a projector into the null-space of the Jabobian, $\boldsymbol{E} \in \mathbb{R}^{n\times n}$ is identity matrix, $\ddot{\boldsymbol{\theta}}_a \in \mathbb{R}^n$ is arbitrary vector with dimension of acceleration. Here, we denote the acceleration set (**??**) as $\mathcal{Q}_J$ and note that all possible solution which ensures constraint (**??**) must belong to $\mathcal{Q}_J$.

3.3.2 Constraint of RNS-C

With considering the kinematic constraint described above, we examine the constraint which the motion under RNS-C must fulfills. The constraint equation of RNS-C is obtained from (**??**) as:

$$\ddot{\boldsymbol{\theta}}^{ref} = -\boldsymbol{M}_{Al}^{+}(\boldsymbol{M}_A\dot{\mathcal{V}}_A + \mathcal{C}_A) + \boldsymbol{M}_{Al}^{+}\boldsymbol{T}\mathcal{F}_B + \boldsymbol{P}_{RNS}\ddot{\boldsymbol{\theta}}_a \tag{3.10}$$

Note that, for the sake of simplicity, we assume that zero gravitational environments or compensating gravity term already. Here, we denote an acceleration set $mathcalQ_{M_{Al}}$ as:

$$\mathcal{Q}_{M_{Al}} = \{\ddot{\boldsymbol{\theta}} \in \mathbb{R}^n | \ddot{\boldsymbol{\theta}} = -\boldsymbol{M}_{Al}^{+}(\boldsymbol{M}_A\dot{\mathcal{V}}_A + \mathcal{C}_A) + \boldsymbol{P}_{RNS}\ddot{\boldsymbol{\theta}}_a\} \tag{3.11}$$

where, this set is composed of acceleration of (**??**) except the constraint force related term. $\mathcal{Q}_{M_{Al}}$ denote the acceleration set which completely free-floating model must satisfy.

Here, we assume the case that there is no constraint forces $\mathcal{F}_b = \boldsymbol{0}$ and $\bar{m}_n$ is not much larger than the inertia parameters of the other links. In this case, because the control model is completely free-floating model and different from the real model, fixed base model, the acceleration to generate desired acceleration of the end-effector differs from $\mathcal{Q}_J$. Hence we say $\mathcal{Q}_{M_{Al}} \neq \mathcal{Q}_J$. By adding an appropriate constraint force, joint accelerations in $\mathcal{Q}_{M_{Al}}$ become a member of the set $\mathcal{Q}_J$ as shown in Fig. **??** (a).

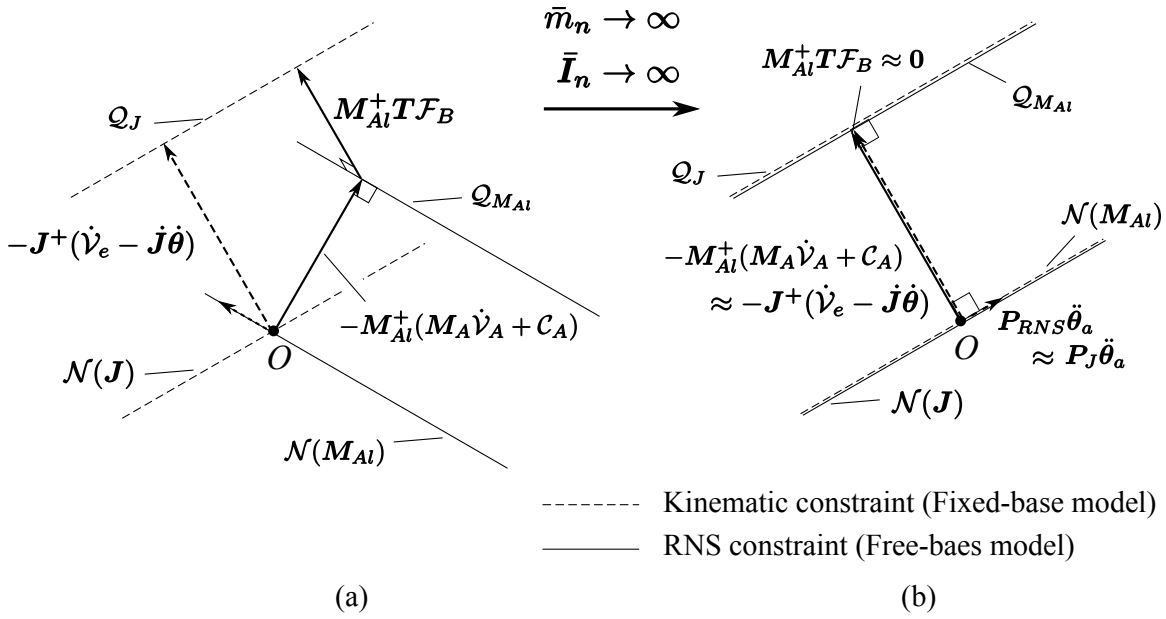

Fig. 3.8: Geometric interpretation of the RNS constraint: (a) right constrained-link's mass and (b) heavy constrained-link's mass.

In contrast to this, in the case of huge inertia of the constrained link, namely $\bar{m}_n \to \infty$, via the momentum conservation law, the linear and angular velocity of the link n becomes zero as:

$$\bar{\boldsymbol{v}}_n = \lim_{\bar{m}_n \to \infty} \frac{1}{\bar{m}_n} \sum_{i=0}^{n-1} \bar{m}_i \bar{\boldsymbol{v}}_i = \boldsymbol{0} \tag{3.12}$$

$$\bar{\boldsymbol{\omega}}_n = \lim_{\bar{\boldsymbol{I}}_n \to \infty} \bar{\boldsymbol{I}}_n^{-1} \sum_{i=0}^{n-1} \{\bar{\boldsymbol{I}}_i \bar{\boldsymbol{\omega}}_i + \bar{m}_i [\bar{\boldsymbol{r}}_i \times] \bar{\boldsymbol{v}}_i\} = \boldsymbol{0} \tag{3.13}$$

Hence, even if there is no constraint force in the system, control model, it means free-floating model, is equivalent to the fixed-base model in the perspective of mechanics. Because the acceleration set which fulfills to generate the desired acceleration of the end-effector is unique in mechanically equivalent model, $\mathcal{Q}_{M_{Al}}$ will close to $\mathcal{Q}_J$ with increasing of the inertia of the constrained link. Therefore, in the case of $\mathcal{Q}_{M_{Al}} \approx \mathcal{Q}_J$, the motion under RNS-C coincides that under RA-C due to the nature of pseudoinverse (minimum norm solution) regardless of the dynamic parameters of the applied model.

In summary, we can conclude that the following:

$$\lim_{\hat{m}_n \to \infty} \boldsymbol{\theta}_{RNS}(t, \bar{m}_n) = \boldsymbol{\theta}_{RA}(t). \tag{3.14}$$

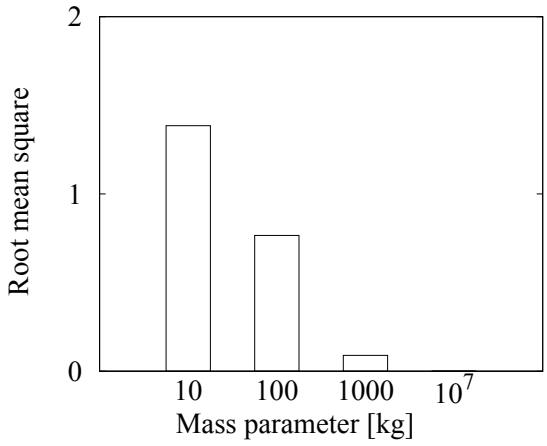

(a)

Fig. 3.9: Root mean square of the joint motion error between the RNS and resolved acceleration (RA).

where, $\boldsymbol{\theta}_{RNS}$, $\boldsymbol{\theta}_{RA} \in \mathbb{R}^n$ are joint motion under RNS-C and RA-C.

3.3.3 Verification via numerical simulations

We verify the fact described above with increasing the inertia of the constrained link via numerical simulations. The applied model is the three-dof planar redundant manipulator and simulation conditions and desired trajectory are same as in Chapter **??**. For evaluation, we adopt root mean square (RMS) of the error vector $\Delta\boldsymbol{\theta} = \boldsymbol{\theta}_{RNS} - \boldsymbol{\theta}_{RA}$ as:

$$\mathrm{RMS}[\Delta\boldsymbol{\theta}(t)] = \sqrt{\frac{1}{t_1 - t_0}\int_{t_0}^{t_1} ||\Delta\boldsymbol{\theta}||^2} \tag{3.15}$$

$$\Delta\theta_i = \theta_{RNSi}(t) - \theta_{RAi}(t) \tag{3.16}$$

The simulation results with some inertia parameters is shown in Fig. **??**. From the results, with increasing the inertia of the constrained link, it can be seen that error vector converge to zero.

Note that motion under inertia-weighted pseudoinverse falls into unstable almost all cases. On the other hand, resolved acceleration control with minimum norm solution is stable compared to inertia-weighted one [18]. Hence if we focus on joint motion, RNS-C has a advantage compared to OS-C.

3.4 Joint stabilization with minimum velocity norm

3.4.1 The relationship between velocity based solution and acceleration base one

One of problems in acceleration control of redundant manipulator is instability of joint motion. It is known that almost all control methods fall into that unstable without global optimization criteria. Therefore, it is important to control redundant motions via appropriate stabilization methods. In particular, in order to execute force control, we have to consider this problem because force control is based of acceleration (or torque) formulations.

In general, for this problem, joint damper technique is usually used. However, in this case, it is difficult to stabilize the joint motion via relatively small gain [14].

In this study, we will provide an stabilization technique via minimum velocity constraint. We can obtain that constraint derived from the time derivation of the velocity (momentum) based solution. Here, generalized momentum conservation law is written in the following form:

$$\boldsymbol{M}_A\mathcal{V}_A + \boldsymbol{M}_{Al}\dot{\boldsymbol{\theta}} = \boldsymbol{0} \tag{3.17}$$

where, we assumed that zero initial momentum, null external forces and zero gravity. From this equation, velocity base redundancy resolution can be obtained via pseudoinverse decomposition as:

$$\dot{\boldsymbol{\theta}} = -\boldsymbol{M}_{Al}^{+}\boldsymbol{M}_A\mathcal{V}_A + \boldsymbol{P}_{RNS}\dot{\boldsymbol{\theta}}_a. \tag{3.18}$$

The first term of r.h.s. in (**??**) obtain minimum velocity norm solution. We can obtain the constraint with time derivation of that term. Note that it is needed a time-derivative of pseudoinverse as described in Appendix **??**.

$$\begin{aligned}\ddot{\boldsymbol{\theta}} =& -\boldsymbol{M}_{Al}^{+}(\boldsymbol{M}_A\dot{\mathcal{V}}_A + \dot{\boldsymbol{M}}_A\mathcal{V}_A + \dot{\boldsymbol{M}}_{Al}\dot{\boldsymbol{\theta}}) \\ & - \boldsymbol{P}_{RNS}\dot{\boldsymbol{M}}_{Al}^{T}(\boldsymbol{M}_{Al}\boldsymbol{M}_{Al}^{T})^{-1}\boldsymbol{M}_A\mathcal{V}_A,\end{aligned} \tag{3.19}$$

Note that the nonlinear force vector $\mathcal{C}_A$ is represented as:

$$\mathcal{C}_A = \dot{\boldsymbol{M}}_A\mathcal{V}_A + \dot{\boldsymbol{M}}_{Al}\dot{\boldsymbol{\theta}} - \frac{\partial T}{\partial \mathcal{X}_A}. \tag{3.20}$$

Hence, formulation (**??**) can be rewritten as:

$$\begin{aligned}\ddot{\boldsymbol{\theta}} =& -\boldsymbol{M}_{Al}^{+}(\boldsymbol{M}_A\dot{\mathcal{V}}_A + \mathcal{C}_A - \frac{\partial T}{\partial \mathcal{X}_A}) \\ & - \boldsymbol{P}_{RNS}\dot{\boldsymbol{M}}_{Al}^{T}(\boldsymbol{M}_{Al}\boldsymbol{M}_{Al}^{T})^{-1}\boldsymbol{M}_A\mathcal{V}_A, . \end{aligned} \tag{3.21}$$

By comparing to (**??**), there are two additional terms in the formulation (**??**). That is the partial derivative of total kinetic energy and an null space acceleration related to motion of the end-effector. Here, in contrast to the null space acceleration, the partial derivation term is appeared because (**??**) only represents only a part of the equation of motion. We will describe the relationship of conservation laws and equation of motion in Appendix **??**.

3.4.2 Simulation study

We verify influences caused by these two additional term via numerical simulations. In order to reveal what term are important for stabilization of joint motion, we conduct following three case:

Minimum velocity norm solution (Case 1)

$$\begin{aligned}\ddot{\boldsymbol{\theta}} =& -\boldsymbol{M}_{Al}^{+}(\boldsymbol{M}_A\dot{\mathcal{V}}_A + \mathcal{C}_A + \frac{\partial T}{\partial \mathcal{X}_A}) + \boldsymbol{M}_{Al}\boldsymbol{T}\mathcal{F}_b \\ & - \boldsymbol{P}_{RNS}\dot{\boldsymbol{M}}_{Al}^{T}(\boldsymbol{M}_{Al}\boldsymbol{M}_{Al}^{T})^{-1}\boldsymbol{M}_A\mathcal{V}_A, \end{aligned} \tag{3.22}$$

Only the null space acceleration term (Case 2)

$$\begin{aligned}\ddot{\boldsymbol{\theta}} =& -\boldsymbol{M}_{Al}^{+}(\boldsymbol{M}_A\dot{\mathcal{V}}_A + \mathcal{C}_A) + \boldsymbol{M}_{Al}\boldsymbol{T}\mathcal{F}_b \\ & - \boldsymbol{P}_{RNS}\dot{\boldsymbol{M}}_{Al}^{T}(\boldsymbol{M}_{Al}\boldsymbol{M}_{Al}^{T})^{-1}\boldsymbol{M}_A\mathcal{V}_A, \end{aligned} \tag{3.23}$$

Only the partial derivative term (Case 3)

$$\ddot{\boldsymbol{\theta}} = -\boldsymbol{M}_{Al}^{+}(\boldsymbol{M}_A\dot{\mathcal{V}}_A + \mathcal{C}_A + \frac{\partial T}{\partial \mathcal{X}_A}) + \boldsymbol{M}_{Al}\boldsymbol{T}\mathcal{F}_b \tag{3.24}$$

In this section, we adopt the three-dof planar redundant manipulator described above as the applied model. Simulation conditions are same as previous simulation. And also the desired trajectory is the circular arc. Note that we adopt an extremely large value, such that 10^6 kg, for the inertia of the constrained link to remove the influence of constraint force.

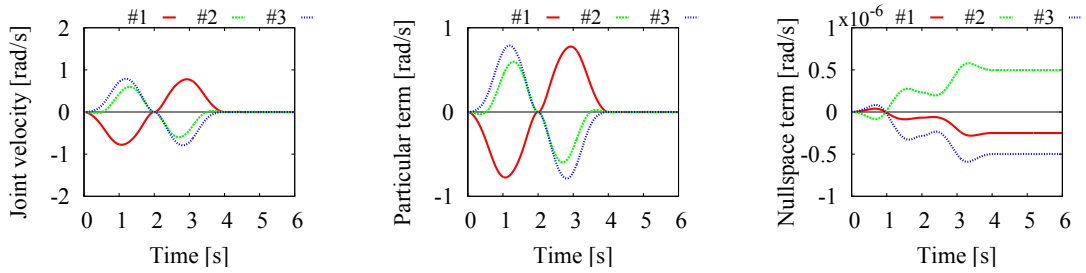

Fig. 3.10: Nullspace stabilization with complete integrability condition (Case 1): The results show that the joint motion coincides minimum velocity norm motion.

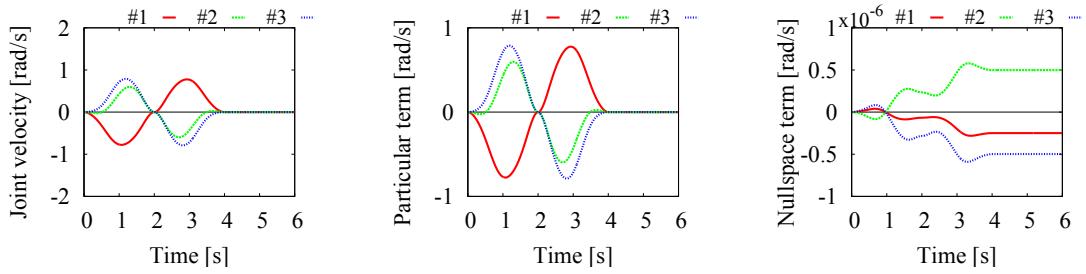

Fig. 3.11: Nullspace stabilization without the partial derivative of total kinetic energy (Case 2): The results show that the joint motion is not influenced by this term.

Verification with Case 1

The simulation results are displayed in Fig. **??**. Besides, in order to examine redundant motion, we docompose joint velocity into two orthogonal components via projector of the Jacobian as:

$$\begin{aligned}\dot{\boldsymbol{\theta}} &= \dot{\boldsymbol{\theta}}_{\perp} + \dot{\boldsymbol{\theta}}_{||} \\ &= (\boldsymbol{E} - \boldsymbol{P}_{RNS})\dot{\boldsymbol{\theta}} + \boldsymbol{P}_{RNS}\dot{\boldsymbol{\theta}}\end{aligned} \tag{3.25}$$

From the results, the order of null space velocity is about 10^{-6}, we can confirm that minimum velocity norm solution can be obtained. Note that this minimum error is caused by the error between $\mathcal{Q}_{M_{Al}}$ and $\mathcal{Q}_J$. Hence, we can reduce this error with increasing the inertia of the constrained link.

Verification with Case 2

We display the results in Fig. **??**. Comparing to the results in case 2, the order of null space velocity is same as in Case 1. Hence, the partial derivative term does not affect the joint motion.

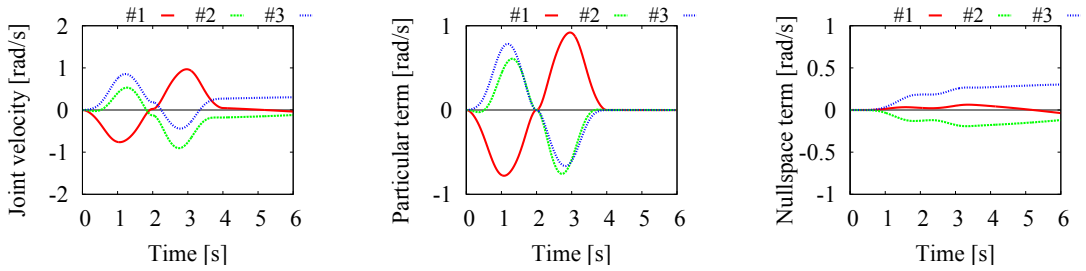

Fig. 3.12: Nullspace stabilization without nullspace acceleration term (Case 3): The results show that nullspace velocity can be observed.

Verification with Case 3

The simulation results are shown in Fig. **??**. In contrast to the above two cases, it can be observed that null space velocity is relatively large order. Hence, from these results, we can conclude that the important term stabilizing null space velocity is the null space acceleration term related to the motion of the end-effector.

In summary, by adding the additional null space acceleration term,

$$\ddot{\boldsymbol{\theta}}_a = -\boldsymbol{P}_{RNS}\dot{\boldsymbol{M}}_{Al}^T(\boldsymbol{M}_{Al}\boldsymbol{M}_{Al}^T)^{-1}\boldsymbol{M}_A\mathcal{V}_A, \tag{3.26}$$

into the original formulation (**??**), we can obtain the motion with approximate minimum velocity norm in hybrid control.

3.5 Summary

In this chapter, we examined joint motion under RNS-C in redundant manipulators. As a result, we can confirm that the inertia of the constrained link affect joint motion behavior through constraint force. In particular, we proved that the motion under RNS-C coincides that under RA-C with huge inertia of the constrained link. This result was confirmed via numerical simulations.

We dealt with joint stabilization problem in redundant manipulators with acceleration based control. For this purpose, we obtained the constraint of minimum velocity norm derived from time derivative of velocity (momentum) based formulation. As a result, if we add an additional null space acceleration term into the original formulation, We can obtained stable joint motion with hybrid motion control.

In the future works, we should deal with the following issues:

- Examine how to affect choice of particular component to multi objective control

•

Bibliography

[1] K. Yoshida, "Engineering test satellite VII flight experiments for space robot dynamics and control: theories on laboratory test beds ten tears ago, now in orbit," *The International Journal of Robotics Research*, vol. 22, no. 5, pp. 321–335, 2003.

[2] Z. Vafa and S. Dubowsky, "On the dynamics of manipulators in space using the virtual manipulator approach," in *Proc. IEEE Int. Conf. Robot. Automat.*, vol. 4, 1987, pp. 579–585.

[3] D. Nenchev, K. Yoshida, and Y. Umetani, "Introduction of redundant arms for manipulation in space," in *IEEE Int. Workshop on Intelligent Robots*, 1988, pp. 679–684.

[4] D. Nenchev and K. Yoshida, "Impact analysis and post-impact motion control issues of a free-floating Space robot subject to a force impulse," *IEEE Trans. Robot. Autom.*, vol. 15, no. 3, pp. 548–557, Jun. 1999.

[5] Y. Masutani, F. Miyazaki, and S. Arimoto, "Sensory feedback control for space manipulators," in *Proc. 1989 Int. Conf. Robot. Automat.*, 1989, pp. 1346–1351.

[6] N. Hara, D. Nenchev, and D. Sato, "Momentum conserving path tracking through dynamic singularities with a flexible-base redundant manipulator," in *Proc. 2010 IEEE/RSJ Int. Conf. on Intelligent Robots and Systems*, 2010, pp. 5392–5397.

[7] T. J. Debus and S. P. Dougherty, "Overview and Performance of the Front-End Robotics Enabling Near-Term Demonstration (FREND) Robotic Arm," in *AIAA Unmanned Unlimited Conference*, 2009, pp. 1–12.

[8] K. Yoshida, K. Hashizume, and S. Abiko, "Zero reaction maneuver: flight validation with ETS-VII space robot and extension to kinematically redundant arm," in *Proc. IEEE Int. Conf. Robot. Automat.*, 2001, pp. 441–446.

[9] M. Oda, K. Kibe, and F. Yamagata, "ETS-VII, space robot in-orbit experiment satellite," in *Proc. IEEE Int. Conf. Robot. Automat.*, vol. 1, 1997, pp. 739–744.

[10] D. N. Nenchev and K. Yoshida, "Singularity-consistent teleoperation techniques for redundant free-flying robots," in *AIAA Guidance, Navigation, and Control Conference,*, 1999, pp. 1895–1902.

[11] K. Yoshida, D. Nenchev, P. Vichitkulsawat, H. Kobayashi, and M. Uchiyama, "Experiments on the PTP operations of a flexible structure mounted manipulator system," *Proc. of IEEE/RSJ Int. Conf. on Intelligent Robots and Systems.*, vol. 1, pp. 246–251, 1996.

[12] G. Gilardi and I. Sharf, "Literature survey of contact dynamics modelling," *Mechanism and Machine Theory*, vol. 37, no. 10, pp. 1213–1239, Oct. 2002.

[13] K. O'Neil and Y.-C. Chen, "Instability of pseudoinverse acceleration control of redundant mechanisms," in *Proc. Int. Conf. Robot. Automat.*, 2000, pp. 2575–2582.

[14] K. O'Neil, "Divergence of linear acceleration-based redundancy resolution schemes," *IEEE Transactions on Robotics and Automation*, vol. 18, no. 4, pp. 625–631, Aug. 2002.

[15] J. Hollerbach, "Redundancy resolution of manipulators through torque optimization," in *Proc. Int. Conf. Robot. Automat.*, 1985, pp. 1016–1021.

[16] O. Khatib, "A unified approach for motion and force control of robot manipulators: The operational space formulation," *IEEE Journal on Robotics and Automation*, vol. 3, no. 1, pp. 43–53, 1987.

[17] H. Bruyninckx and O. Khatib, "Gauss' principle and the dynamics of redundant and constrained manipulators," in *Proc. Int. Conf. Robot. Automat.*, 2000, pp. 2563–2568.

[18] J. Hollerbach, "Local versus global torque optimization of redundant manipulators," in *Proc. Int. Conf. Robot. Automat.*, 1987, pp. 619–624.